

## Article

# Sedimentary Facies Types and Their Control of Reservoirs in the Lower Jurassic Lacustrine Facies Shale of the Lianggaoshan Formation, Northeastern Sichuan Basin, China

Chao Ni <sup>1</sup>, Xueju Lv <sup>1,\*</sup>, Xinjian Zhu <sup>1</sup>, Jianyong Zhang <sup>1</sup>, Jiahao Wang <sup>2</sup>, Mingyang Wang <sup>2</sup> and Ruibin Xu <sup>2</sup><sup>1</sup> PetroChina Hangzhou Research Institute of Geology, Hangzhou 310023, China<sup>2</sup> School of Earth Resources, China University of Geosciences (Wuhan), Wuhan 430074, China

\* Correspondence: lvxj\_hz@petrochina.com.cn

**Abstract:** In recent years, new breakthroughs have been made in the field of shale oil and gas exploration in the Lower Jurassic Lianggaoshan Formation in Sichuan Basin. At present, there is a lack of systematic studies on reservoir properties and sedimentary facies of the Lianggaoshan Formation shale. Therefore, in this study, taking the Lianggaoshan Formation in Sichuan Basin as an example, the sedimentary facies types of shale reservoirs and their control over shale oil and gas are systematically studied, based on a large number of outcrops, experimental testing, logging, and seismic interpretation methods. The results show that five sedimentary microfacies are developed in the Lianggaoshan Formation in the study area, namely, semi-deep lake mud, shallow lake mud, wave-influenced shallow lake mud, delta-influenced shallow lake mud, and underwater interbranch bay microfacies. The stratum thickness of the Lianggaoshan Formation is in the range of 26–315 m, and mainly distributed in the eastern region, but rapidly thinned in the northwestern region. The sedimentary sequence framework of the Lianggaoshan Formation has been constructed. Moreover, the lithology of the Lianggaoshan Formation shale has been divided into three types, including shale, massive mudstone and silty mudstone. The brittleness index and total organic carbon (TOC) value of three types of shale show a negative correlation. Silty mudstone has the highest brittleness, while that of black shale is the lowest. For porosity and permeability, massive mudstone is better than silty mudstone, and silty mudstone is better than black shale. There are many kinds of matrix pores in the Lianggaoshan Formation shale, and the development degree of inorganic pores is higher than that of organic pores. Finally, based on the analysis of oil-bearing, pore types, physical properties and productivity, it is considered that black shale facies is the most favorable lithofacies type. The deep–semi-deep lacustrine facies belt obviously controls the shale oil enrichment of the Lianggaoshan Formation.

**Keywords:** Sichuan Basin; Lower Jurassic; Lianggaoshan Formation; shale; sedimentary facies belt; productivity



**Citation:** Ni, C.; Lv, X.; Zhu, X.; Zhang, J.; Wang, J.; Wang, M.; Xu, R. Sedimentary Facies Types and Their Control of Reservoirs in the Lower Jurassic Lacustrine Facies Shale of the Lianggaoshan Formation, Northeastern Sichuan Basin, China. *Processes* **2023**, *11*, 2463. <https://doi.org/10.3390/pr11082463>

Academic Editor: Junqian Li

Received: 20 July 2023

Revised: 5 August 2023

Accepted: 8 August 2023

Published: 16 August 2023



**Copyright:** © 2023 by the authors. Licensee MDPI, Basel, Switzerland. This article is an open access article distributed under the terms and conditions of the Creative Commons Attribution (CC BY) license (<https://creativecommons.org/licenses/by/4.0/>).

## 1. Introduction

Tapping into the potential of shale oil and gas resources in continental lacustrine basins is an important development direction of oilfield exploration in China [1–4]. The organic shale in continental lacustrine basins of China is widely distributed in the Permian and Neogene depositional systems, and has good prospects for shale oil exploration [5–10]. China has already realized the scale construction and production of continental shale oil in many exploration areas of different basins, for example, the Permian Lucaogou Formation in the Junggar Basin, Jimusa'er Depression, the Chang 7 Member of the Upper Triassic in the Ordos Basin, the Cretaceous Qingshankou Formation in the Songliao Basin, and the Paleogene in the Cangdong Depression in the Bohai Bay Basin [11–17].

More and more researchers pay attention to the effect of sedimentary microfacies of shale reservoir quality [4,18]. A large number of studies have shown that differences in the

sedimentary microfacies of shale affect TOC content, mineral composition, diagenesis and pore structure, and thus affect the quality of the shale reservoir [19–22]. Previous studies on sedimentary microfacies of shale mainly focused on marine shale, but there are few studies on sedimentary microfacies of continental oil shale. Therefore, the classification of sedimentary microfacies of continental oil shale and its influence on reservoir quality has become a new hotspot.

The Lower Jurassic Lianggaoshan Formation in the Sichuan Basin is a new oil and gas exploration layer that was discovered in recent years. Therefore, the reports on the geological study of the Lianggaoshan Formation shale are very limited. In particular, the study of sedimentary facies classification of the Lianggaoshan Formation is still a research gap. The Lower Jurassic Lianggaoshan Formation in the Sichuan Basin, China, has seen some new breakthroughs in shale oil and gas exploration in recent years. The discovery of industrial oil and gas flows from several wells in the Pingchang, Yuanba and Fuling areas confirms the huge exploration potential of lacustrine shale oil in the formation. For example, in the middle and lower part of the Lianggaoshan Formation, Well Ping'an 1 (or Well PA1) in the Yilong-Pingchang area has a daily oil production of 112.8 m<sup>3</sup> and a daily gas production of 11.45 × 10<sup>4</sup> m<sup>3</sup>.

At present, some basic studies have been carried out under the sedimentary sequence framework, on tectonic evolution and resource potential of shale oil and gas in the Lianggaoshan Formation [23–25]. However, there are few studies on micro-reservoir properties, sedimentary microfacies types and their influencing factors on Lianggaoshan Formation shales. Similar to the sedimentary environment of the Lianggaoshan Formation shales, lacustrine shales also developed in the early Paleogene in China.

In this study, taking the Lianggaoshan Formation in Sichuan Basin as an example, the sedimentary facies types of shale reservoirs and their control over shale oil and gas are systematically studied, based on a large number of outcrops, experimental testing, logging, and seismic interpretation methods. This study is of great significance to the rapid development of continental shale oil and gas exploration in Sichuan Basin.

## 2. Materials and Methods

In this study, the outcrops of six profiles and 582 m cores of 13 wells (Ping'an 1, Xiqian 1, Yuntan 1, Tailiu 1, Gong 17, Gong 30, Xi 56, Xi 20, Longqian 102, Longqian 2, Gong 17, Xian 9 and Guang 100) of the Lower Jurassic Lianggaoshan Formation in the Sichuan Basin (Figure 1) are systematically observed. Meanwhile, 1273 samples including shale, mudstone and silt mudstone were obtained from six wells. These samples are used for lithofacies type analysis, organic geochemical testing, and reservoir quantitative characterization. The experimental results, including thin section, scanning electron microscope, X-ray diffraction and physical property experiments, are used to evaluate the petrology, physical property, pore development and sedimentary facies of the organic-rich strata in the Lianggaoshan Formation.

An Imager.D2m microscope was used to observe the microscopic structures of the mineral. An X Pert ProX-ray diffractometer was used to examine the mineral composition inside the samples. The test conditions were as follows: CuK $\alpha$  radiation was used; the transmitting slit and scattering slit were both 1°, and the receiving slit was 0.3°; the pipe pressure was 40 Kv; the pipe flow was 40 mA. Moreover, the particle size of the sample was  $\varnothing \leq 0.075$  mm. A carbon and sulfur analyzer, LECO CS-230, was used to analyze the content of organic matter; all the samples were ground into fine powder smaller than 200  $\mu$ m, and they were treated with hydrochloric acid for 24 h to remove carbonate minerals in the samples. Then, the organic carbon of the samples was completely oxidized into carbon dioxide by heating it to 900 °C.

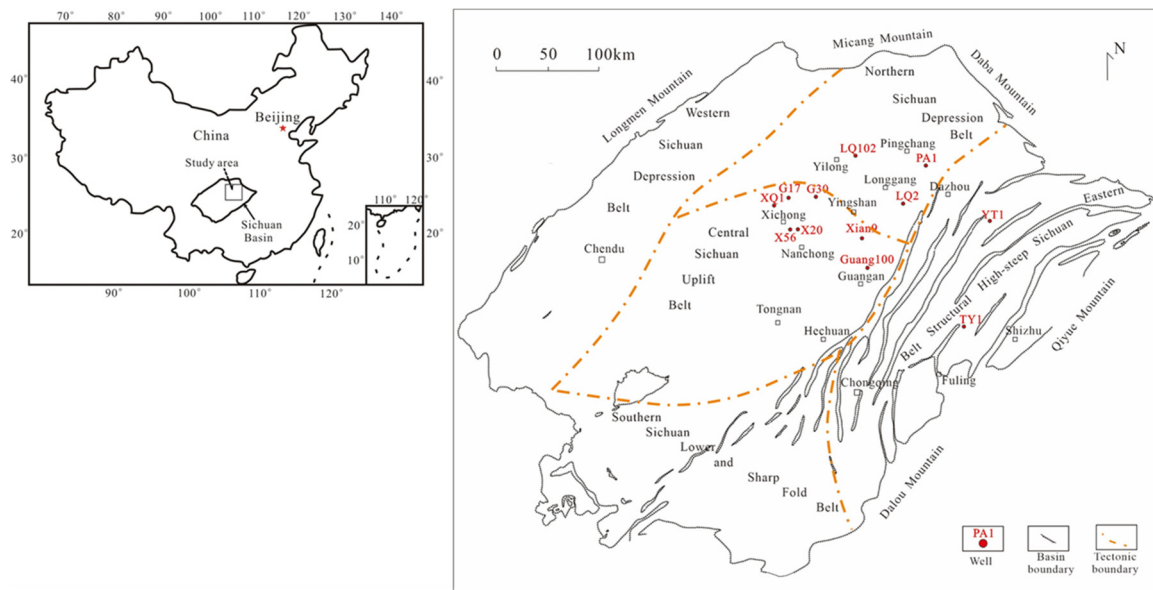


**Figure 1.** Location map of Sichuan Basin displaying the studied wells.

A combined overburden gas porosity and permeability tester, FYKS-3, was used to measure the porosity and permeability of the samples. All the samples were cylindrical with a diameter of 2.5 cm and length of 3 cm. The porosity of shale was obtained via the helium porosity test method [26–28]. The permeability of shale was carried out via the pulse attenuation method, and the test standard used was “GB/T 29172-2012 Core Analysis Method” [29]. The gas medium used was high-purity nitrogen with a confining pressure of 1500 psi.

In addition, Apreo S was used to perform SEM observations. An oil and gas evaluation workstation was used to perform pyrolytic analysis using the rock pyrolytic, Analysis Method GB/T18602-2001 [30]. The pyrolysis experiment was carried out on the shale processed into 60~80 meshes. Semi-closed hydrocarbon generation and expulsion simulation were used in the thermal simulation experiment. In the analysis of the composition of the thermal simulation products, analysis was carried out in accordance with the oil and gas industry standard SY/T5118-200 [31].

A carbon–sulfur analyzer was used to determine the total organic carbon content of shale. The shale samples were ground to a particle size of less than 0.2 mm and 1 mol/L of hydrochloric acid was added to remove the inorganic carbon from the samples. The shale samples were then fed into a high-temperature carbon–sulfur analyzer to determine the CO<sub>2</sub> and SO<sub>2</sub> levels based on the light intensity absorbed by the gas. The total organic carbon content of the shale sample could be obtained by dividing the carbon and sulfur content of the two kinds of gas by the mass of the shale sample.

The logging parameters used included natural gamma (GR), acoustic wave time difference (AC), rock density (DEN), RT (resistivity), and RXO (flush zone resistivity), and M2RX (array-induced resistivity). These parameters are used to analyze the lithology and quality of a target reservoir [32]. The research results can provide a scientific basis for evaluating the shale oil potential of the Lianggaoshan Formation in Sichuan Basin.

### 3. Geological Background

During the Middle and Late Triassic, with the closing of the Mianluo Ocean and the uplift of the Qinling Orogenic Belt, the main part of the Sichuan Basin ended the history of marine deposition and began to receive continental clastic deposition since the Late Triassic [23]. The Lower and Middle Jurassic continental sediments include the Lower Jurassic Ziliujing Formation (J<sub>1z</sub>), the Middle Jurassic Lianggaoshan Formation (J<sub>2l</sub>) and the

Middle Jurassic Shaximiao Formation (J<sub>2s</sub>) [23]. The lacustrine shales are well-developed in the Middle Jurassic Lianggaoshan Formation.

According to the principle of sequence stratigraphy and the characteristics of marker layers, three lacustrine basin development periods have been identified in the Lianggaoshan Formation. Then, the Lianggaoshan Formation is divided into the first, second and third Liang segments (Figure 2). Furthermore, the Lianggaoshan Formation is divided into eight stratigraphic units, corresponding to eight stages of basin development and evolution (Figure 2). There are three, two and three substratigraphic units in the first, second and third member, respectively (Figure 2). The eight depositional units are distributed in the whole basin, and there is no pinch out or truncation of the strata. In addition, the average porosity and permeability of the Lianggaoshan Formation shales are 4% and 0.18 mD, respectively.

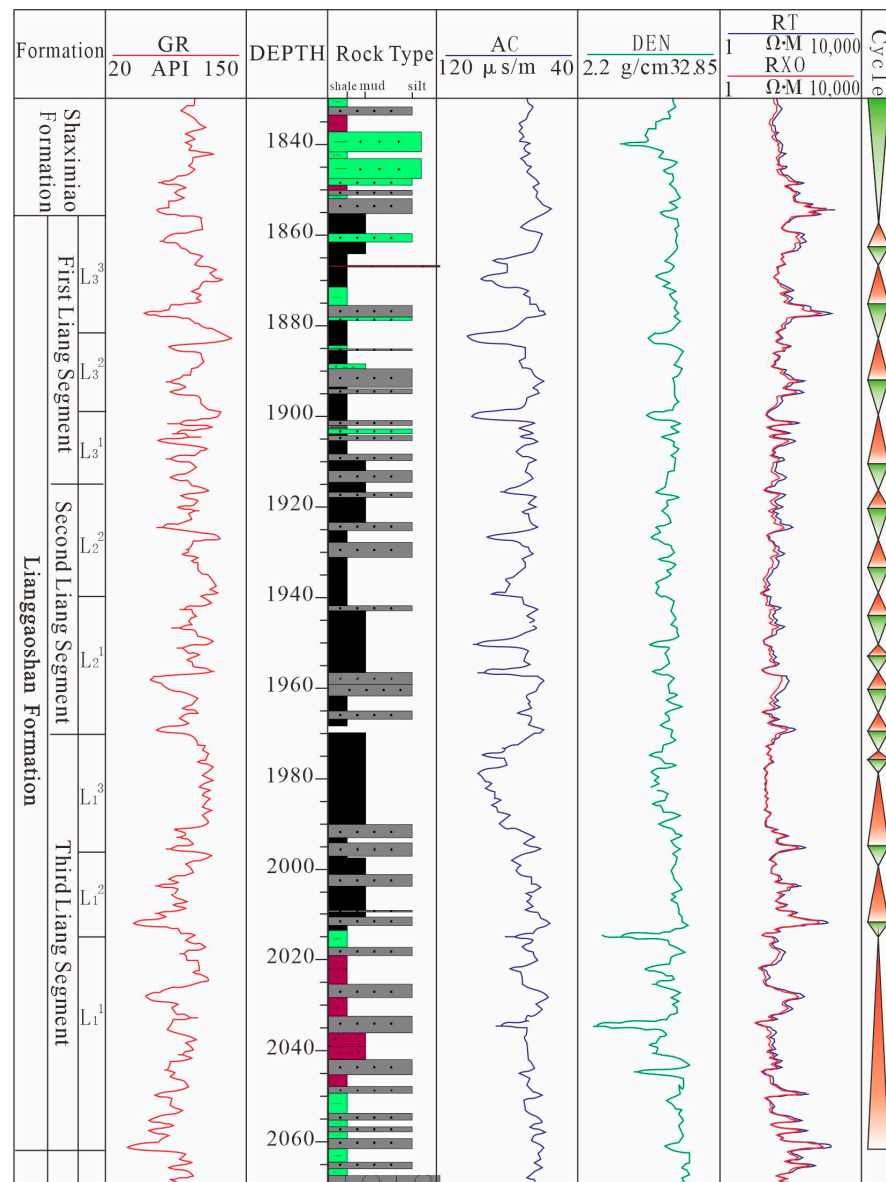
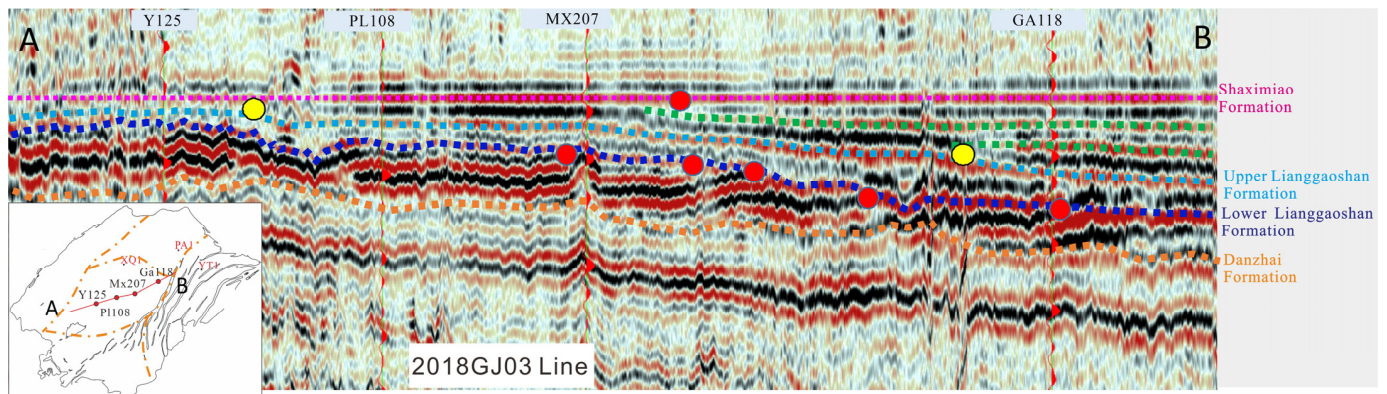


**Figure 2.** Division of depositional units of Lianggaoshan Formation in Well Longqian 2. GR: natural gamma; AC: acoustic wave time difference; DEN: rock density; RT: resistivity; RXO: flush zone resistivity.

## 4. Results

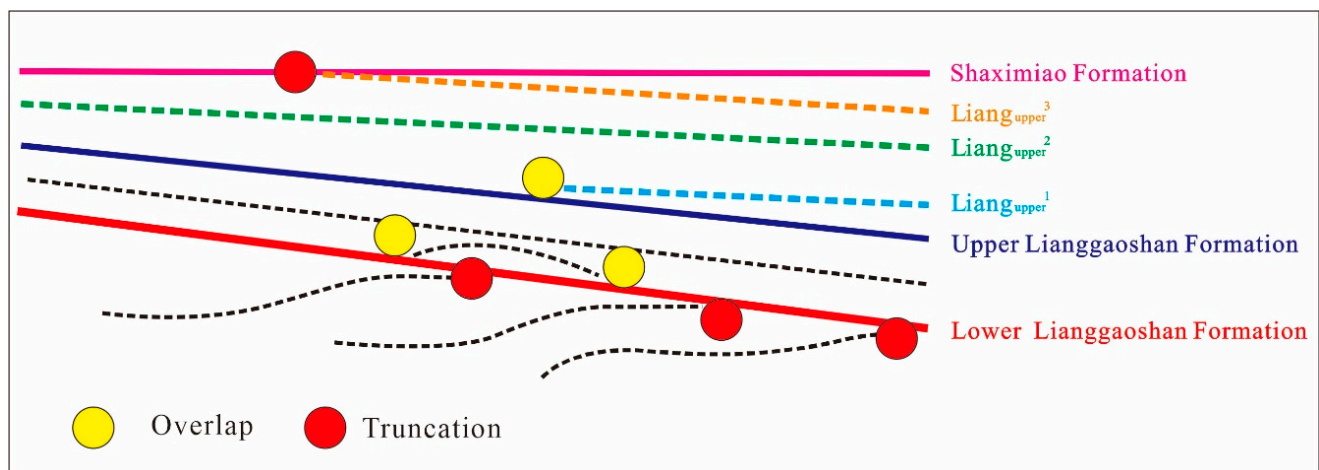
### 4.1. Sedimentary Sequence Framework

Figure 3 shows the spatial characteristics of the sedimentary stratigraphic framework revealed by the 2018 GJ03 seismic line. The bottom of Lianggaoshan Formation is a truncated unconformity. The lower strata are lost via denudation, and the denudation degree of the strata to the northeast is gradually increased. This indicates that after the underlying strata were deposited, the northern strata were gradually flattened by uplift and erosion [33–36].



**Figure 3.** Interpretation of the stratigraphic framework of the Lianggaoshan Formation (seismic line AB shown in Figure).

The lower and upper segments of the Lianggaoshan Formation have different seismic reflections, and correspond to a third-order sequence, respectively (Figure 4). The lower segment has weak intermittent reflection (corresponding to drilling variegated lithology), and the upper segment has a strong-amplitude continuous reflection (as a deeper water body lake basin, namely the shale oil exploration horizon). The top surface of the Lianggaoshan Formation is a truncated unconformity surface, and the erosion degree of the stratum is increased to the southwest. The thickness of the lower member of the Lianggaoshan Formation is relatively stable in the whole area, while the upper member presents a south–west thinning wedge shape (Figure 4).



**Figure 4.** Seismic reflection structure of the Lianggaoshan Formation, Sichuan Basin, China.

The stratum thickness of the Lianggaoshan Formation ranges from 26 to 315 m, and it is mainly distributed in the east, but it thins greatly toward the northwest. The thickness of the lower member of the Lianggaoshan Formation is 25–113 m, and the distribution of the strata is uniform, generally being at 50–80 m. The thicker strata are located in the northeastern part of the basin, but the distribution range is small.

Recent shale reservoir drilling in the northeastern part of the basin has revealed good shale reservoirs and production capacity. The sedimentary thickness of the Lianggaoshan Formation in this area is large, which represents the subsidence and the sedimentary center of the basin during the syndepositional period.

#### 4.2. Sedimentary Facies Type of Shale Reservoirs

The sedimentary microfacies of shale has been seldom investigated in the previous studies. Combined with field outcrops and core observations, it is found that the shale of the Lianggaoshan Formation in the study area developed five sedimentary microfacies: namely, semi-deep lake mud, shallow lake mud, wave-influenced shallow lake mud, delta-influenced shallow lake mud, and underwater interbranch bay microfacies. The varieties of sedimentary facies are reflected in the location of the paleo-sedimentary environment, lithologic association and sedimentary structures.

##### (1) Underwater interbranch bay microfacies

The interbranch bay develops in the low-lying area between the finger-like distributary channels. Due to river blocking on both sides, the hydrodynamic force is weak, and dark gray shale is developed. The well-developed siltstone lamina, block-horizontal bedding and deformation structures can be found locally. Moreover, its thickness is generally <1 m, and the maximum is 4 m. The underwater interbranch bay microfacies are usually sandwiched between the point sand bar and the underwater distributary channel microfacies, or between the underwater distributary channel microfacies. The shale is dark in color, mostly dark gray-black, and has a high content of organic carbon.

For example, the interbranch bay microfacies in the 2157.86–2164.12 m interval of Well Yuntanyi 1 consists of dark gray-gray black shales. Gray laminae and a large number of fossil shell organisms (bivalve) can be found, and a small number of gastropod fossils are seen in the upper part of the shale (lighter color, lower TOC content). Horizontal laminae, calcareous laminae (saline water) and fossil organisms are developed in some areas, indicating favorable source sedimentary environments. The results show that the TOC content of most samples is more than 2%, and that of some samples can reach 3%. The S1 of most samples is >1 mg/g, and some samples are >2 mg/g. Oil immersion is found in some local fractures.

##### (2) Shallow lake mud microfacies

The shallow lake is in the range of a low-water-level lake to a normal-weather-wave base level during the dry season [37–41]. The shallow lake mud microfacies were formed in the environment of weak wave action and far away from the delta. They usually consist of dark gray shale and have a developed horizontal bedding. Compared with other shallow lacustrine micro-facies, this kind of shale contains less siltstone laminae. However, there are abundant bivalves, a few gastropod fossils and a few burrows. These fossils indicate a shallow lacustrine sedimentary background and are significantly different from the semi-deep lacustrine mud microfacies (Figure 5).

##### (3) Shallow lake mud microfacies affected by waves or deltas

This microfacies is composed of dark gray shale with siltstone laminae or interlayers, and horizontal, wavy and lenticular beddings. A large number of small individual burrows and disturbed structures were discovered. Siltstone laminae and biological burrows are the signs of distinguishing shallow lacustrine facies from semi-deep lacustrine facies. Siltstone laminae or interlayers contribute more to the reservoir performance of shale oil. According to the source of the siltstone lamina, the shallow lake microfacies are divided into two

types: the shallow lake affected by waves and the shallow lake affected by deltas. Figure 6 shows the core photos of the 2433.94–2441.22 m well section in Well Xiqian 1. It represents the shallow lake mud microfacies affected by the delta, and is composed of dark gray shale with -layer siltstone thin laminae and shell limestone. Moreover, the corresponding log curves are usually of a low-amplitude weak tooth funnel type.



**Figure 5.** Jinwocun profile. There are a lot of bivalve fossils in the shallow lacustrine shale of the Lianggaoshan Formation.

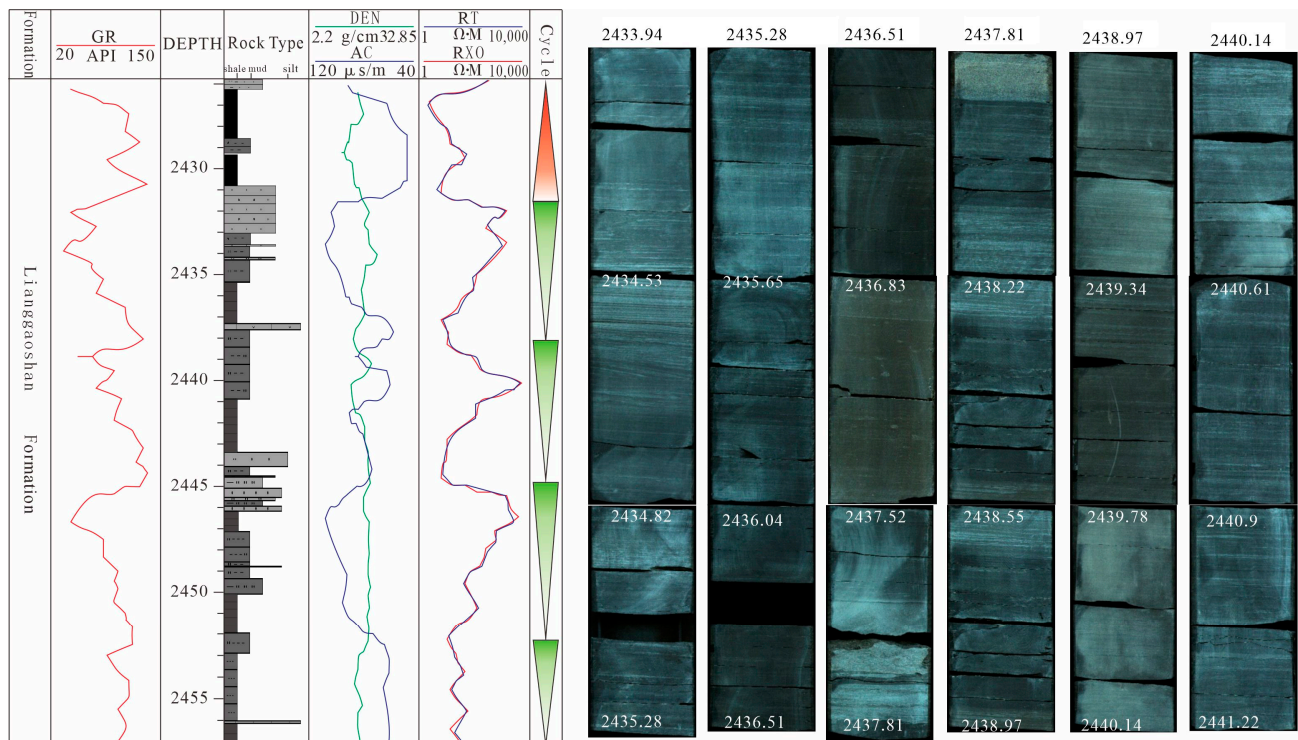


**Figure 6.** Development characteristics of 2433.94–2441.22 m cores in Well Xiqian 1. They reveal the sedimentary characteristics of the shallow lacustrine mud microfacies affected by the delta. GR: natural gamma; DEN: rock density; RT: resistivity; RXO: flush zone resistivity.

(4) Semi-deep lake mud microfacies

The semi-deep lake is the transition type from a shallow lake to deep lake, and the energy of the water body is weak. This kind of sedimentary microfacies is mainly composed of grey-black shale, and has the characteristics of a deep color, being pure (without siltstone), well-developed shales, no fossils and a lower GR amplitude (with a higher GR value). Its

characteristics are obviously different from those of shallow lake mud microfacies. Among them, the bedding appears as a thin layer ( $1\text{ mm}\pm$ ) and flat surface with great brittleness (Figure 7A–D).

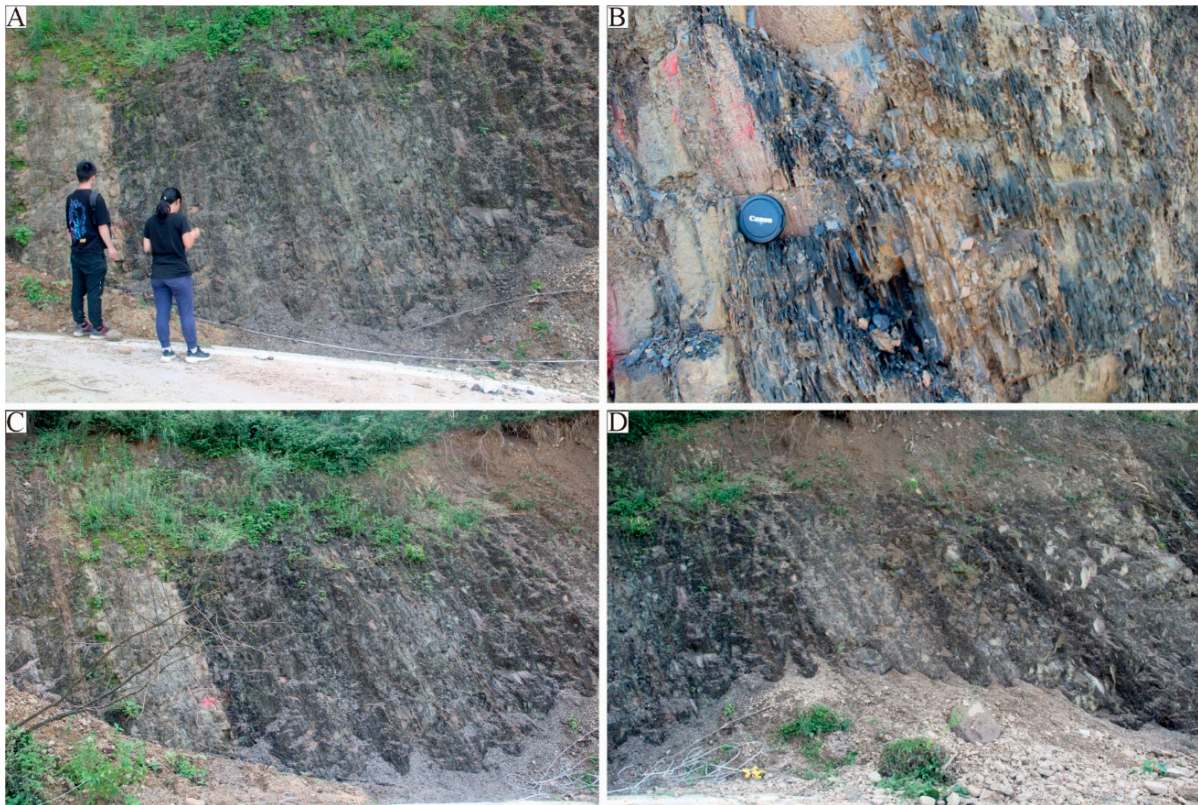


**Figure 7.** Jinwocun outcrop profile. Semi-deep lacustrine shale deposits in the upper member of the Lianggaoshan Formation.

#### 4.3. Petrological Characteristics of Shale Reservoirs

The microscopic identifications of the core and cast thin sections show that the main rock types of the Lianggaoshan Formation are shale and siltstone; in addition, a small amount of shell limestone is developed (Figure 8).

In this study, Lianggaoshan Formation shale is divided into three types, including shale, massive mudstone and silty mudstone (Figure 9). There are obvious different types of shale under a microscope. The color of black shale is dark and the lamina is well-developed. Dark minerals such as clay minerals, feldspar and quartz are interbedded (Figure 9a–c). Moreover, the high content of bitumen in the pores indicates the property of good oil-bearing [42–44]. In contrast, massive mudstones are generally homogeneous (Figure 9d) and lack lamellar development. The mineral composition mainly includes clay minerals, and the content of feldspar and quartz is obviously smaller (average value of 51.1%). The content of felsic minerals in silty mudstone is relatively higher with an average value of 55.2%, and the color is lighter [45–47]. Felsic minerals are more obvious and the bitumen content is smaller in the fluorescent thin section (Figure 9e,f). This reflects the poor oil-bearing capacity of shale [18,48–51].

The whole-rock X-ray diffraction data show that the black shale type is mainly felsic shale. The content of dolomite/calcareous carbonate in shale is relatively low, but the content of some samples is about 12%, the content of clay mineral is 40~60%, and the brittleness index is 40~60%. Taking Well Xiqian 1 as an example, it can be seen that the clay mineral content and brittleness index of different shale types are slightly different (Figure 10).

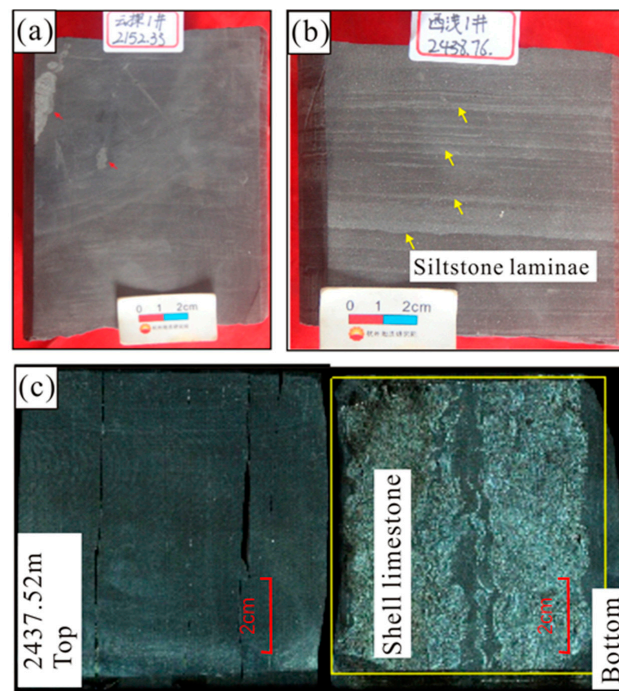


**Figure 8.** Photos of different lithologic cores of the Lianggaoshan Formation in the study area. Notes: (a) Well YT1, 2152.35 m, dark gray shale; (b) Well XQ1, 2438.76 m, siltstone with laminate structure; (c) Well XQ1, 2437.52 m, black shale and shell limestone.

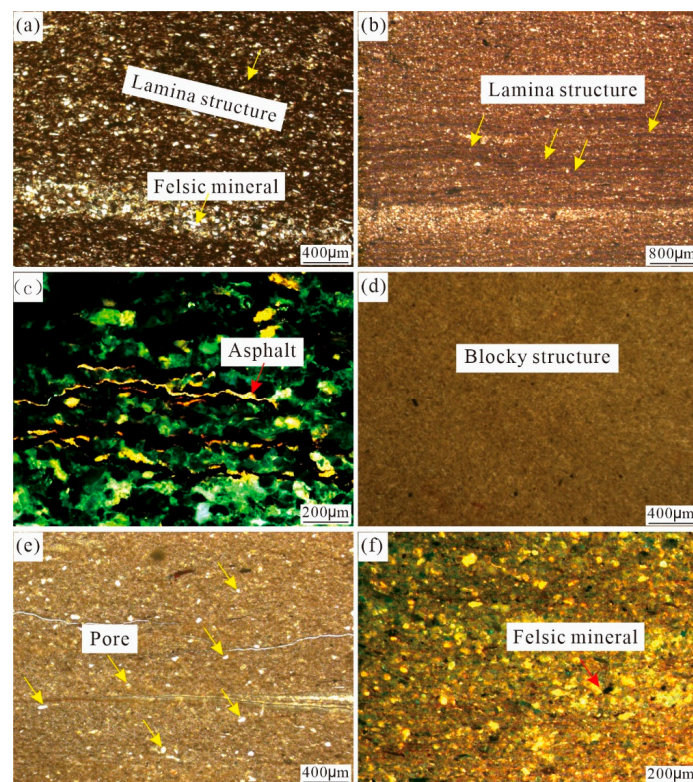


**Figure 9.** Microscopic photographs of the Lianggaoshan shale formation in Sichuan Basin, China. Notes: (a) Well Xiqian 1, 2439.38 m, black shale; interbedded clay minerals, feldspar and quartz. (b) Well Yuntan 1, 2161.42 m, black shale. (c) Well Xiqian 1, 2435.63 m, black shale, fluorescent thin section (d) Well Xiqian 1, 2442.75 m, massive mudstone. (e) Well Xiqian 1, 2435.63 m, silty mudstone. (f) Well Yuntan 1, 2152.23 m, silty mudstone.

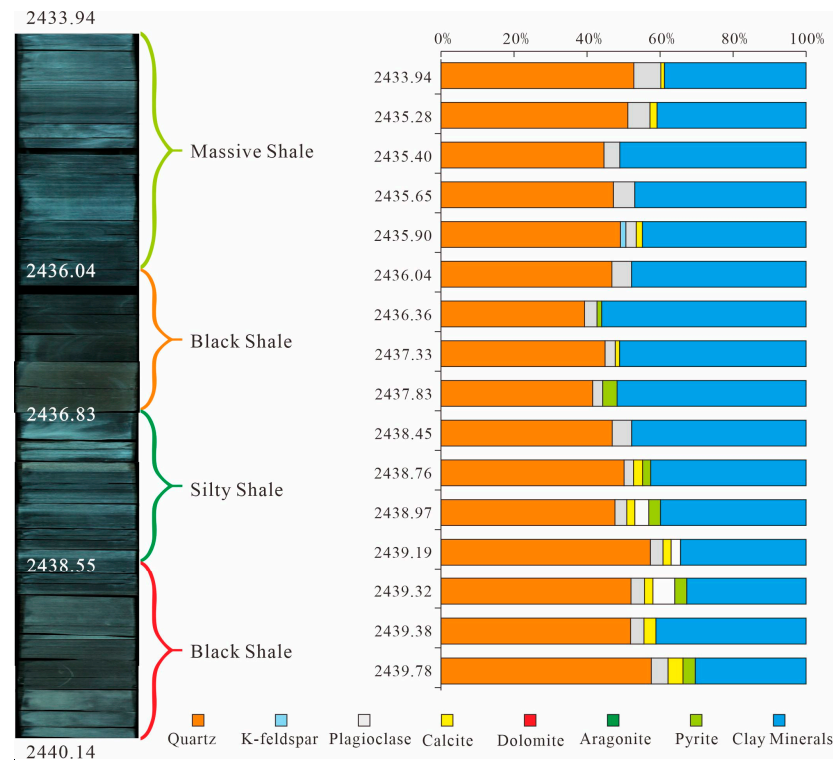


**Figure 10.** Distribution of total rock mineral composition of Lianggaoshan Formation shale in Well Xiqian 1.

Figure 11 shows the relationship between TOC content and quartz content in the target shale. There was a negative correlation between the brittleness index and TOC value. The lower the brittleness index was, the higher the TOC value was. On the whole, the brittleness of silty mudstone is greater than that of massive mudstone, and that of massive mudstone is greater than that of black shale [52–56]. This is mainly due to the relatively low content of felsic minerals in black shale (average value of 42.6%), which makes it less brittle than massive mudstone (average value of 51.1%) and silty mudstone (average value of 55.2%) (Figure 11).

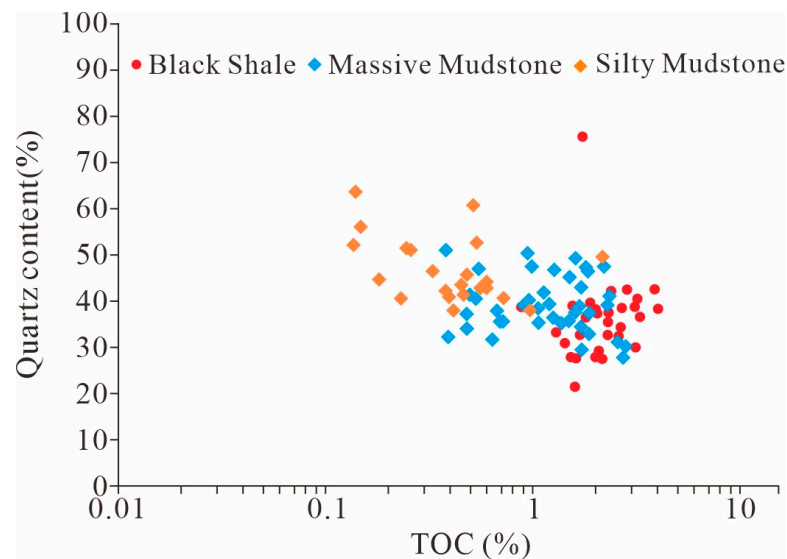


**Figure 11.** Relationship between TOC and quartz content in shale of Lianggaoshan Formation.

#### 4.4. Physical Properties of Shale Reservoirs

In the past, Jurassic reservoirs in Sichuan Basin were mainly explored for limestone, but the research on and understanding of shale is very low. The physical properties of shale in the Lianggaoshan Formation of Well Xiqian 1 are tested in this paper. For massive mudstone with horizontal bedding, the porosity ranges from 1.85% to 6.04%, with an average of 4.9% (Figure 12a). The porosity of silty laminar shale ranges from 2.11% to 5.35%, with an average of 4.0% (Figure 12b). In addition, the porosity of pure black shale ranges from 0.87 to 5.02%, with an average of 3.4% (Figure 12c). The results show that Lianggaoshan Formation shale has reservoir potential.

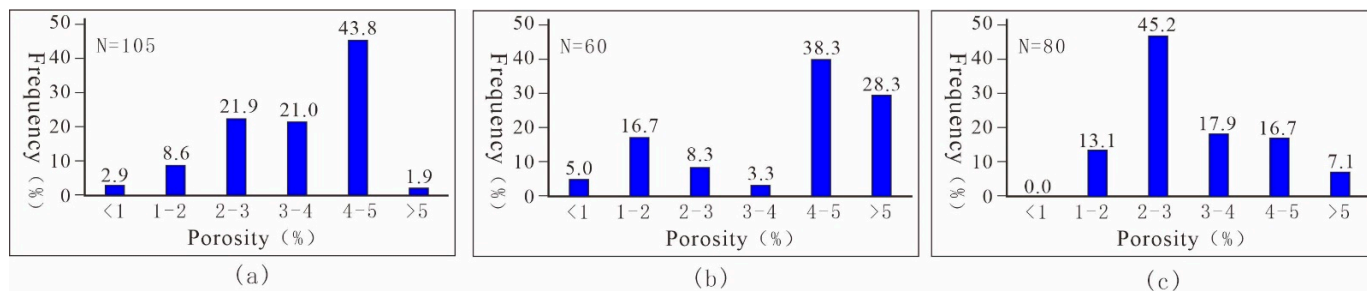


**Figure 12.** Physical properties of different types of shale in Lianggaoshan Formation. Notes: (a) black shale; (b) massive mudstone; (c) silty mudstone.

The brittleness index of black shales is usually lower than that of other shales. However, for shale, when the content of brittle minerals is greater than 30%, the criteria of the sweet-spot reservoir can be satisfied. For a physical property, it is usually one of the reference standards for a shale sweet spot, but for Lianggaoshan Formation black shale, not all shale samples have low porosity. It can be seen from Figure 11 that the major interval of porosity of the black shale samples is greater than 4%, and this type of shale has reservoir potential.

#### 4.5. Pore Types

From the scanning electron microscope analysis results, it can be seen that micropores are developed in the shale of the Lianggaoshan Formation in Sichuan Basin. According to the origin of matrix pores, they can be divided into organic matter pores, secondary dissolution pores, intercrystalline pores, mineral mold pores and clay mineral micropores. According to the statistics, inorganic pores are more developed than organic pores are [57–59]. This may be related to the low degree of thermal evolution of organic matter in the shale of the Lianggaoshan Formation in the Sichuan Basin.

The pore types of shale in the Lianggaoshan Formation in Sichuan Basin are divided into primary pores and secondary pores. The primary pores are subdivided into intercrystalline micro-nano-pores and intergranular micro-nano-pores.

##### (1) Intercrystalline micro-nano-pores

The primary intercrystalline pores are mainly clay mineral, pyrite and gypsum intercrystalline pores (Figure 13a–d). These types of pores are well-developed in black-brown-black shale, followed by the gray-black massive mudstone.

Intercrystalline pores of clay minerals are formed via the accumulation or directional arrangement of clay minerals [60–63]. Most of these pores are formed during diagenesis, and the flakey clay minerals are oriented and deformed due to pressure and tectonic compression. According to the SEM images, the pores of this type are usually slit-shaped, wedge-shaped or triangular (Figure 13a,b). The pore size can be 20–30 nm, the slit-shaped length can be extended to 5–20  $\mu\text{m}$ , and the connectivity is good. This type of pore is often associated with organic matter (Figure 13a,b).

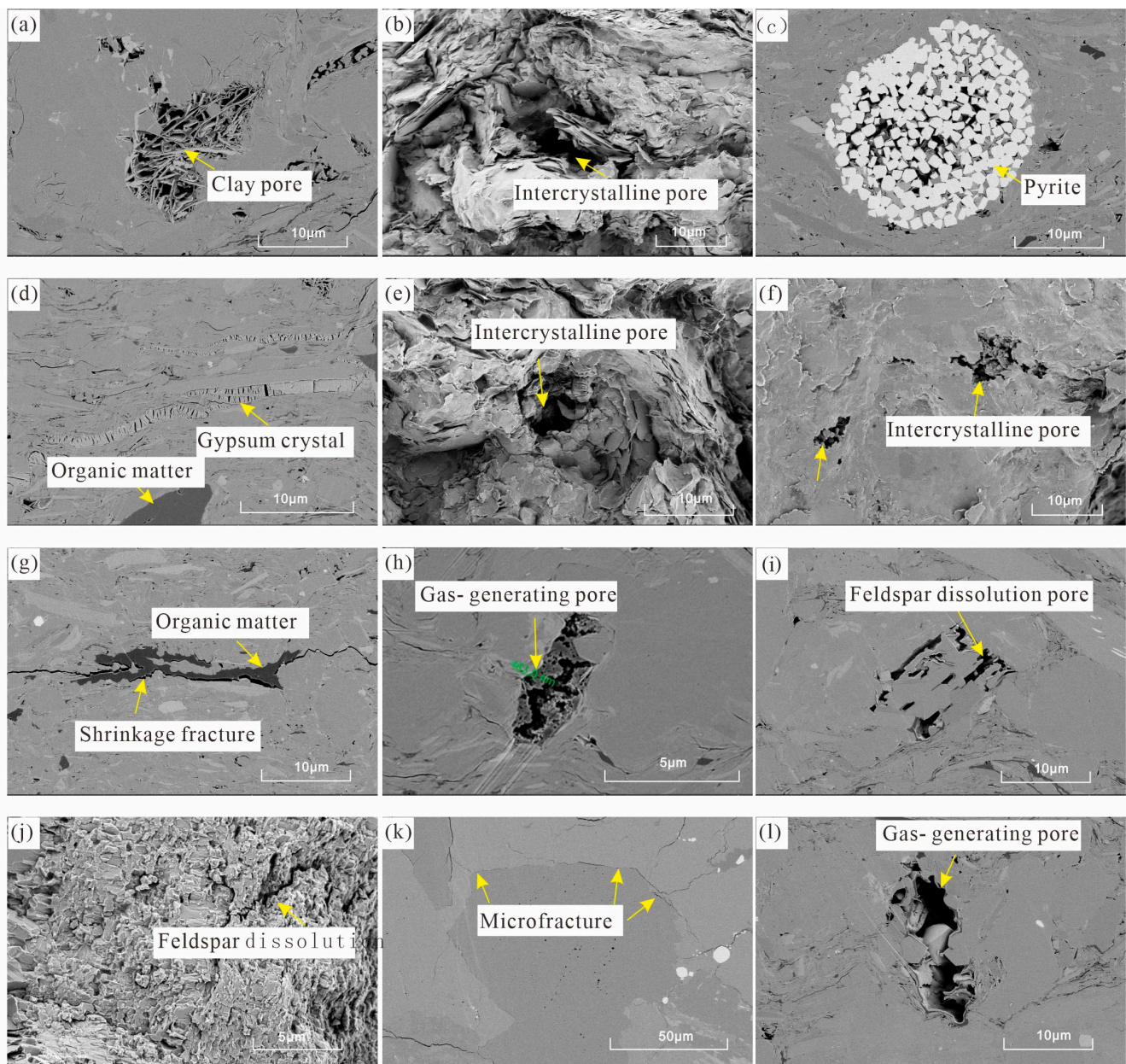


**Figure 13.** Scanning electron microscope (SEM) photographs of the target shale reservoirs. Notes: (a) Well Xiqian 1, 2439.38 m, clay mineral pores partially filled with asphalt; (b) Well Yuntan 1, 2164.8 m, intercrystalline pore; (c) Well Xiqian 1, 2159.48 m, pyrite intercrystalline pores filled with organic matter; (d) Well Xi56, 1679.1 m, gypsum and organic matter intercrystalline pores; (e) Well Xiqian 1, 2435.9 m, intergranular pores; (f) Well Xiqian 1, 2435.9 m, intergranular pores; (g) Well Xiqian 1, 2437.83 m, massive mudstone and organic matter shrinkage fractures; (h) Well Gong 21, 2264.3 m, gas-generating pores; (i) Well Xiqian 1, 2439.38 m, feldspar dissolution pores; (j) Well Xiqian 1, 2437.81 m, feldspar dissolution pores; (k) Well Xiqian 1, 2437.81 m, intergranular fractures of brittle minerals; (l) Well Xiqian 1, 2439.38 m, gas-generating pores.

The existence of intercrystalline pores in pyrite indicates the reduction environment [64–66]. Pyrite intercrystalline pores usually develop between pyrite crystals and are often associated with organic matter (Figure 13c). In addition, gypsum has been found in the target shale. Some intercrystalline pores are also developed in gypsum and indicate a strong reduction environment (Figure 13d).

## (2) Intergranular micro-nano-pores

Primary intergranular pores are the pores formed via the accumulation of primitive clastic particles [67–69]. They are mainly formed via the anti-compaction or pre-compaction of brittle minerals such as quartz and feldspar. Intergranular pores of organic plasmids or microbial cavities can also be formed in some granular organic matter (Figure 13e,f). Some intergranular pores develop where plastic particles bend around rigid particles and are preserved under the shelter of rigid particles. However, some intergranular pores are preserved through rigid particles supporting each other. The SEM images show that the intergranular pores are nearly triangular, cylindrical and wedge-shaped, with a wide distribution of 30 nm~2 μm.

Secondary pores are divided into organic gas-generating pores and dissolution pores.

### (1) Organic gas-generating pores

Organic gas-generating pores are the residual pores formed via hydrocarbon generation. These pores are usually elliptic, flaky or irregular in shape. In addition, organic-matter particles shrink in size during hydrocarbon generation, resulting in shrinkage gaps in organic matter or between organic matter and inorganic minerals (Figure 13g,h). The pore diameter of organic gas-generating pores is 20 nm~500 μm.

### (2) Dissolution pores

Secondary solution pores are pores of different sizes and irregular shapes produced via the dissolution of minerals during diagenesis [70–73]. The dissolution pores of the target shale are mainly feldspar dissolution pores (Figure 13i,j), with pore sizes ranging from 1 to 5 μm. There are few pores in the single mineral and the connectivity is poor. Feldspar dissolution pores are more developed in black shale and less developed in massive mudstone. This may be related to the dissolution strength of organic acids.

In addition, a large number of microfractures are well-developed in the target layer. Interlayer fracture refers to the micro-fractures along sedimentary bedding caused by geological action. Bedding fractures are greatly affected by tectonic stress, and the shale itself easily fractures along the bedding (Figure 13k,l).

## 5. Discussion

### 5.1. Control of Lithofacies Types on Hydrocarbon Enrichment in Shale

During the sedimentary period of the Lianggaoshan Formation, the Sichuan Basin was compressed by the Daba Mountains Orogenic Belt in the northeast of China. At this time, the Sichuan Basin presents the deep northeast, shallow southwest asymmetry of the foreland basin. The slope of the northeast basin's margin is relatively large, and the provenance supply is more abundant. Then, the basin is a broad shallow lake basin. There are a few semi-deep lakes and deep lakes in the center of the depression, which is surrounded by extensive shallow water areas. Therefore, the dark shales developed in the Jurassic are less thick (Figure 14).

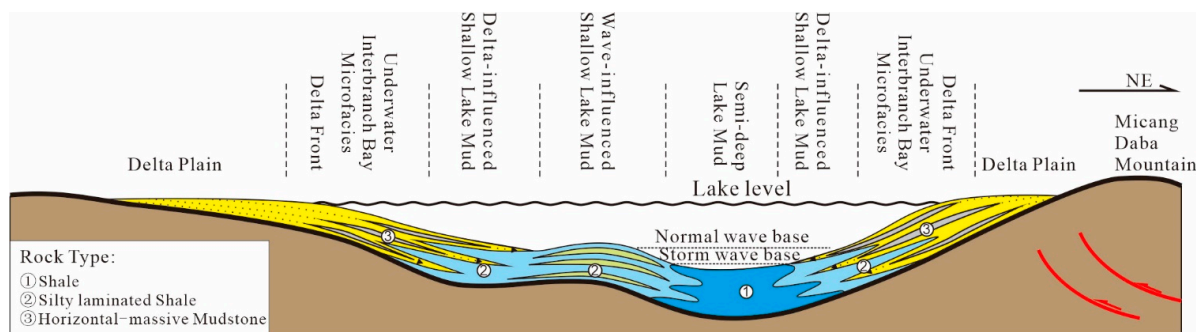


**Figure 14.** Sedimentary model of the Lower Jurassic Lianggaoshan Formation shale in Sichuan Basin, China.

Semi-deep lacustrine facies are developed in the Longgang-Yingshan area of the central Sichuan Basin. The semi-deep lacustrine facies extend in the NNW–SSE direction (i.e., parallel to the northeastern basin’s margin), indicating a northeast compression during this period. The broad and gentle palaeogeomorphologic background and shallow lake water depth condition are favorable for the development of large-area shoal bars in the basin. Affected by the supply of material sources around, the delta was pushed forward toward the interior of the basin. Furthermore, the pure black shale facies are developed under the condition of semi-deep lake shale microfacies. In silty laminar shale, the shale is frequently intercalated with silty sandstone laminar. They are usually developed in the front of a delta and on both sides of shoal bars, that is, delta-influenced and wave-influenced shallow lake mud microfacies.

By analyzing the reservoir characteristics of different types of lithofacies in the shale of the Lianggaoshan Formation, the results show that the black shale facies is the most favorable lithofacies type. It has good oil-bearing capacity, fluid mobility, compressibility and reservoir properties. The maximal TOC content of black shale is over 2%, and the distribution of the TOC isoline of the Lianggaoshan Formation in the Sichuan Basin is shown in Figure 15. There is a good agreement between the TOC content and S1 value. The high-value areas of TOC and S1 are distributed in the middle and north of the basin, including two high-value areas in the south and the north. This area is dumbbell-shaped. It is obvious that the dumbbell-shaped distribution is caused by the long-distance accretion of two large deltas.

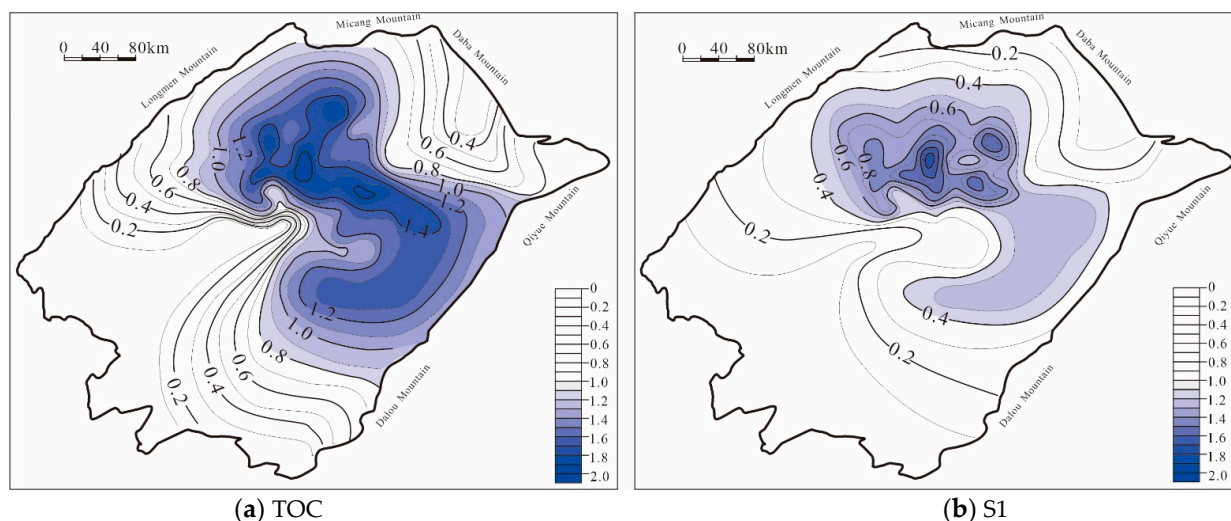


**Figure 15.** Planar distribution of TOC and S1 in the upper submember of the Lianggaoshan Formation, Sichuan Basin, China. Notes: (a) TOC contents; (b) S1.

The microscopic features and organic geochemical analysis show that black shale facies has the best oil-bearing property among the three types of lithology. Calcite and dolomite are well-developed in some shales, so they are highly brittle. These carbonate minerals are more conducive to artificial fracturing than is quartz. The results of physical property tests show that the porosity of black shale is greater than 2%. Moreover, the pore radius is generally above 100 nm, which is favorable for the flow of hydrocarbons [74]. Its reservoir performance and fluid mobility are obviously better than that of massive mudstone.

Combined with exploration practice, the black shale in the Lianggaoshan Formation of Well Ping’an 1 has high productivity; the daily oil Production  $112.8 \text{ m}^3$  and daily gas production  $11.45 \times 10^4 \text{ m}^3$ . Until January, 2022, after 174 days of production, the well an accumulated oil production of  $3536 \text{ m}^3$  and gas production of  $418 \times 10^4 \text{ m}^3$ . At the same time, the black shale of the Lianggaoshan Formation in Well Taiye 1 produces  $9.84 \text{ m}^3$  of oil and  $7.5 \times 10^4 \text{ m}^3$  of gas per day. According to statistics, the high-yield wells of the Lianggaoshan Formation in the Sichuan Basin are characterized by a high content of TOC,

high porosity and a high content of brittle minerals. Therefore, shale facies is the material base of oil and gas enrichment in the Lianggaoshan Formation shale.

5.2. Control of Deep–Semi-Deep Lacustrine Facies Belt on Hydrocarbon Enrichment in Shale

High-quality source rock is the material base of shale oil enrichment. The development of lacustrine organic shale is obviously controlled by the sedimentary facies belt. From the point of view of the sedimentary process, the mechanical and chemical differentiation caused by the hydrodynamic conditions of the lake basin restricts the migration and accumulation of source clasts and organic matter. On the one hand, during the transition from a shoal lake and a shallow lake into a semi-deep lake, the sand content of lithologic assemblage gradually decreased, and the clay mineral content gradually increased. On the other hand, the enrichment of terrigenous parent material usually has obvious regional zonation characteristics. In the delta facies of the shoal lake, inertinite and vitrinite are mainly enriched, while in the shallow and semi-deep lacustrine facies, chitinite are mainly controlled by a gravity flow depositional system, and in the deep lacustrine facies, the ultramicroscopic components are mainly enriched. In addition, the quality of shale in different facies zones is greatly different, which is controlled by the difference in terrigenous clastic and hydrocarbon-generating parent materials. The TOC content, porosity and gas content of semi-deep and deep lacustrine shale are higher than those of lacustrine and shallow lacustrine shale. Therefore, the shale of semi-deep and deep lacustrine facies has the material basis and reservoir space for hydrocarbon enrichment.

In addition, the porosity and gas-bearing property of different-lithology shales in the Lianggaoshan Formation are different according to the results of the gas-bearing tests and reservoir property evaluation. The black shale with a high TOC content (about 2% on average) has a relatively higher porosity (about 5%) and gas content, while the silty mudstone with a low TOC content has relatively poor physical properties and gas content (Figure 16).

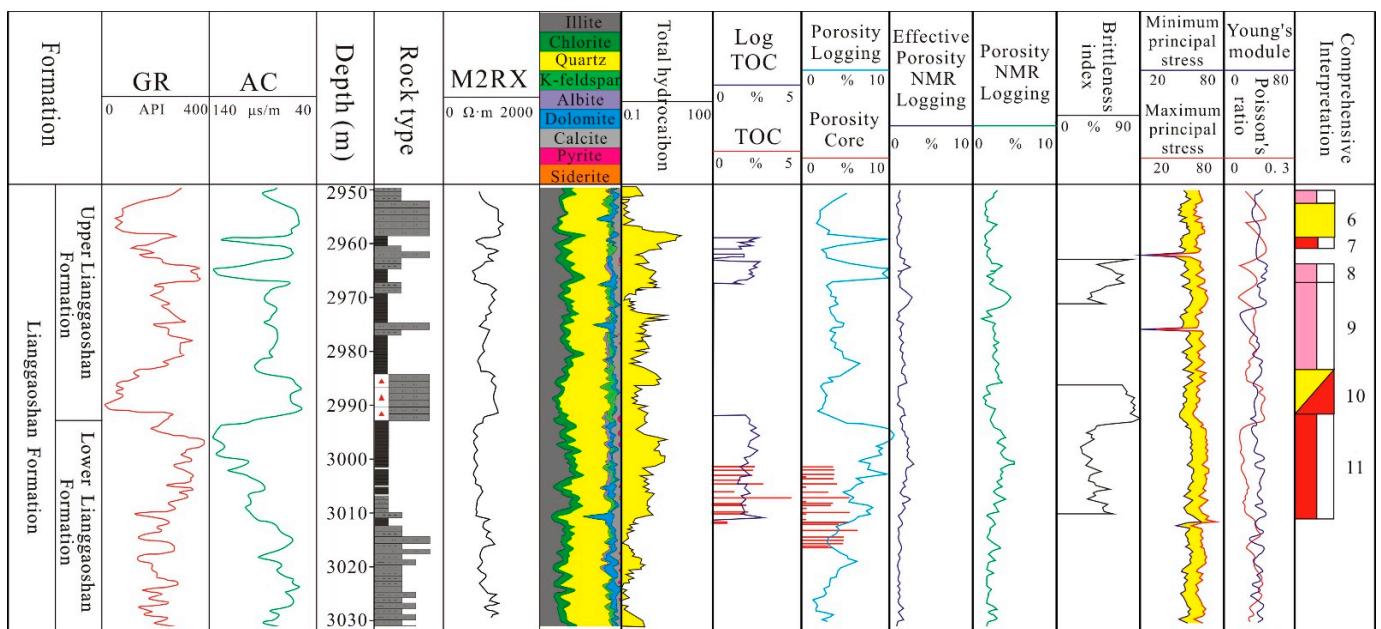


**Figure 16.** Comprehensive log interpretation histogram of Lianggaoshan Formation in Well Ping'an 1. GR—natural gamma; AC—acoustic wave time difference; M2RX—array induced resistivity; TOC—total organic carbon. The logging parameters GR, AC and M2RX were obtained from conventional logging tests. TOC logging values were obtained via the ΔLogR method. NMR porosity and effective porosity were obtained via the nuclear magnetic resonance logging method. In the last track, layer No. 6 is gas layer, layers No. 7 and 11 are oil layers, layers No. 8 and 9 are poor-oil layers, and layer No. 10 layer an oil-gas layer.

The sedimentary environment of deep–semi-deep lacustrine facies is a favorable facies belt for shale facies and hydrocarbon accumulation. Among the lithologic assemblages of the thick-bed shale type, interlayer type and interbedded type, the thick-bed shale type is the most favorable lithofacies assemblage type. For example, the thickness of thick-bed shale in Well Ping’an 1 is 18.9 m (Figure 16). The well has good shale oil and gas production capacity.

On the other hand, the thick shale type usually has good roof and floor conditions. For example, a thick set of siltstones is developed at the top of the oil-rich shale in Well Ping’an 1 (Figure 16). Previously, siltstones were often used as reservoirs. However, this study shows that the physical properties of the Lianggaoshan Formation siltstones are significantly worse than those of the shale, generally because the siltstones are tight in the study area, while the organic pores in the shale are developed. In addition, from the log interpretation, the porosity of the Lianggaoshan Formation siltstone is lower than that of the shale (Figure 16). Therefore, based on the capillary principle, liquid hydrocarbons are not easily injected into siltstones with lower porosity.

According to the production of oil, gas and water in Well Ping’an 1, oil is mainly produced in pure black shale. However, the oil production of the sandstone section is obviously low, and it mainly produces gas. This is mainly due to the relatively small volume of natural gas, which flows more easily than crude oil does during the discharge process (Figure 17). The comprehensive analysis in this study shows that the shale oil of the Lianggaoshan Formation has good preservation conditions, and the deep–semi-deep lake facies is the most favorable facies zone for shale oil enrichment.

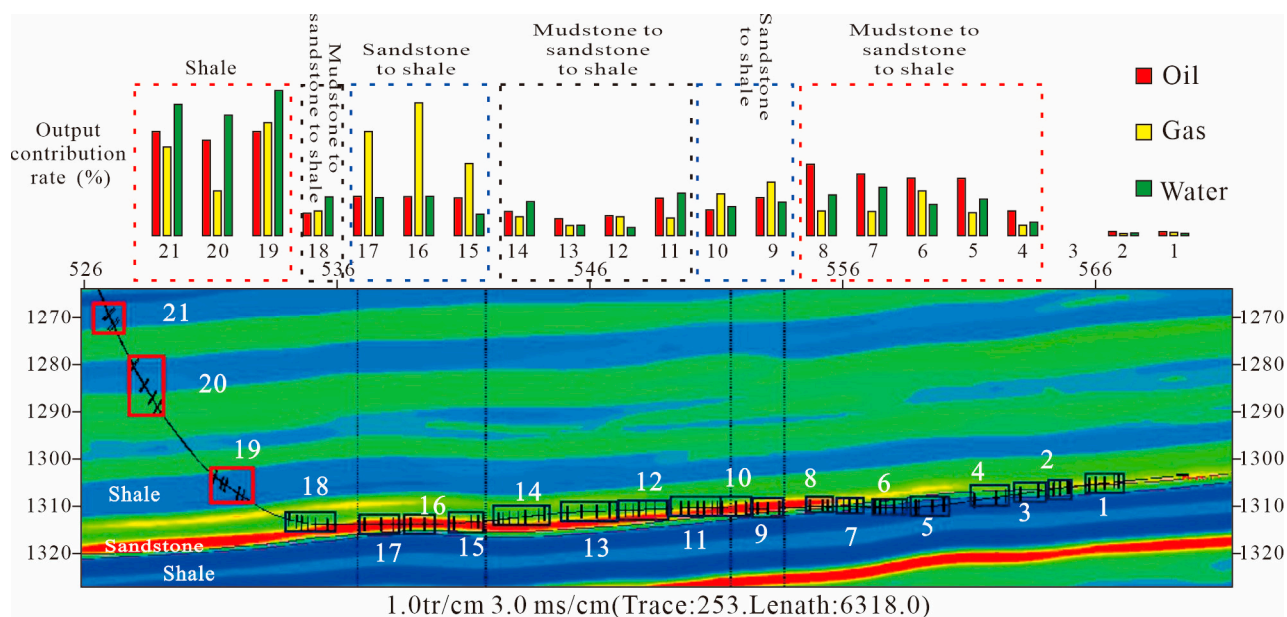


Figure 17. Production profile of oil, gas and water in Well Ping’an 1 (According to He et al., 2022 [24]).

## 6. Conclusions

(1) The stratum thickness of the Lianggaoshan Formation in the Sichuan Basin is in the range of 26–315 m, and it is mainly distributed in the eastern region, but rapidly thins in the northwestern region. The sedimentary sequence framework of the Lianggaoshan Formation has been constructed, and it can be divided into lower and upper segments. Moreover, the lithology of the Lianggaoshan Formation shale has been divided into three types: black shale, massive mudstone and silty mudstone.

(2) The brittleness index and TOC value of the shales show a negative correlation; the lower the brittleness index, the higher the TOC value. Silty mudstone has the highest brittleness, while black shale has the lowest. For physical properties, massive mudstone is better than silty mudstone, and silty mudstone is better than black shale. The development

degree of inorganic pores is higher than that of organic pores. The major interval of porosity of the black shale samples is greater than 4%.

(3) Combined with field outcrops and core observations, it is found that the shale of Lianggaoshan Formation in the study area is developed in five sedimentary microfacies: namely, semi-deep lake mud, shallow lake mud, wave-influenced shallow lake mud, delta-influenced shallow lake mud, and underwater interbranch bay microfacies.

(4) Finally, based on the analysis of oil-bearing, pore types, physical properties and productivity, it is considered that black shale facies is the most favorable lithofacies type. The deep–semi-deep lacustrine facies belt obviously controls the shale oil enrichment of the Lianggaoshan Formation.

**Author Contributions:** Conceptualization, C.N.; Methodology, C.N., X.L., X.Z. and J.W.; Software, X.L., X.Z., M.W. and R.X.; Investigation, C.N., X.L., X.Z., J.Z., J.W., M.W. and R.X.; Resources, C.N. and J.Z.; Data curation, X.L., X.Z., J.W. and M.W.; Writing—original draft, C.N.; Writing—review & editing, X.L., X.Z. and J.Z.; Supervision, C.N. and J.Z.; Project administration, J.Z.; Funding acquisition, J.Z. All authors have read and agreed to the published version of the manuscript.

**Funding:** This work was funded by the Scientific Research and Technology Development Project of PetroChina Company Limited: 2021DJ0501.

**Institutional Review Board Statement:** Not applicable.

**Informed Consent Statement:** Not applicable.

**Data Availability Statement:** Not applicable.

**Acknowledgments:** The authors appreciate the Petro China Southwest Oil & Gasfield Company for supplying the studied samples and providing the original geological data. We are also grateful to the editors and reviewers for providing constructive and careful comments that significantly improved the manuscript.

**Conflicts of Interest:** The authors declare no conflict of interest.

## References

- Chen, S.B.; Zhu, Y.M.; Wang, H.Y. Structure characteristics and accumulation significance of nanopores in Longmaxi shale gas reservoir in the southern Sichuan Basin. *J. China Coal Soc.* **2012**, *37*, 438–444. [\[CrossRef\]](#)
- Chen, Y.; Tang, H.M.; Liao, J.J. Analysis of shale pore characteristics and controlling factors based on variation of buried depth in the Longmaxi Formation, Southern Sichuan Basin. *Geol. China* **2022**, *49*, 472–484. [\[CrossRef\]](#)
- Cui, C.L.; Dong, Z.G.; Wu, D.S. Rock mechanics study and fracability evaluation for Longmaxi Formation of Baoj ing block in Hunan Province. *Nat. Gas Geosci.* **2019**, *30*, 626–634. [\[CrossRef\]](#)
- Zou, X.Y.; Li, X.Q.; Wang, Y. Reservoir characteristics and gas content of Wufeng-Longmaxi formations deep shale in southern Sichuan Basin. *Nat. Gas Geosci.* **2022**, *33*, 654–665. [\[CrossRef\]](#)
- Fan, R.; Zhou, H.; Cai, K. Carbon isotopic geochemistry and origin of natural gases in the southern part of the western Sichuan Depression. *Acta Geosci. Sin.* **2005**, *26*, 157–162. [\[CrossRef\]](#)
- Gao, C.; Meng, S.; Zhang, J.; Wang, J.; Sun, Y. Effects of cementation on physical properties of clastic rock-originated weathering crust reservoirs in the Kexia region, Junggar Basin, NW China. *Energy Geosci.* **2023**, *4*, 74–82. [\[CrossRef\]](#)
- Li, Y. Mechanics and fracturing techniques of deep shale from the Sichuan Basin, SW China. *Energy Geosci.* **2021**, *2*, 1–9. [\[CrossRef\]](#)
- Li, H.; Zhou, J.L.; Mou, X.Y.; Guo, H.X.; Wang, X.X.; An, H.Y.; Mo, Q.W.; Long, H.Y.; Dang, C.X.; Wu, J.F.; et al. Pore structure and fractal characteristics of the marine shale of the Longmaxi Formation in the Changning Area, Southern Sichuan Basin, China. *Front. Earth Sci.* **2022**, *10*, 1018274. [\[CrossRef\]](#)
- Xue, F.; Liu, X.; Wang, T. Research on anchoring effect of jointed rock mass based on 3D printing and digital speckle technology. *J. Min. Strat. Control Eng.* **2021**, *3*, 023013. [\[CrossRef\]](#)
- Zhao, W.; Bian, C.; Xu, Z. Similarities and differences between natural gas accumulations in Sulige gas field in Ordos Basin and Xujiahe gas field in central Sichuan Basin. *Pet. Explor. Dev.* **2013**, *40*, 400–406. [\[CrossRef\]](#)
- Guo, H.; Ji, M.; Sun, Z.; Zhou, Z. Energy evolution characteristics of red sandstone under cyclic load. *J. Min. Strat. Control Eng.* **2021**, *3*, 043019. [\[CrossRef\]](#)
- Liao, F.; Yu, C.; Wu, W. Stable carbon and hydrogen isotopes of natural gas from the Zhongba Gasfield in the Sichuan Basin and implication for gas-source correlation. *Nat. Gas Geosci.* **2014**, *25*, 79–86. [\[CrossRef\]](#)
- Lan, S.R.; Song, D.Z.; Li, Z.L.; Liu, Y. Experimental study on acoustic emission characteristics of fault slip process based on damage factor. *J. Min. Strat. Control Eng.* **2021**, *3*, 033024. [\[CrossRef\]](#)

14. Wan, M.; Xie, B.; Chen, S.; Zou, C.; Zhang, Q.; Ran, Y. Hydrocarbon source correlation of the upper Triassic reservoirs in the Sichuan Basin. *Nat. Gas Ind.* **2012**, *32*, 22–24.
15. Yin, S.; Lv, D.W.; Ding, W.L. New method for assessing microfracture stress sensitivity in tight sandstone reservoirs based on acoustic experiments. *Int. J. Geomech.* **2018**, *18*, 04018008. [[CrossRef](#)]
16. Yin, S.; Wu, Z. Geomechanical simulation of low-order fracture of tight sandstone. *Mar. Pet. Geol.* **2020**, *117*, 104359. [[CrossRef](#)]
17. Yin, S.; Tian, T.; Wu, Z.; Li, Q. Developmental characteristics and distribution law of fractures in a tight sandstone reservoir in a low-amplitude tectonic zone, eastern Ordos Basin, China. *Geol. J.* **2020**, *55*, 1546–1562. [[CrossRef](#)]
18. Zhang, L.; Liu, D.; Gao, Y.J.; Zhang, M. Geochemical Characteristics of Gas and Flowback Water in Lake Facies Shale: A Case Study From the Junggar Basin, China. *Front. Earth Sci.* **2021**, *9*, 635893. [[CrossRef](#)]
19. Mustafa, A.; Tariq, Z.; Mahmoud, M.; Radwan, A.; Abdurraheem, A.; Abouelresh, M. Data-driven machine learning approach to predict mineralogy of organic-rich shales: An example from Qusaiba Shale, Rub’al Khali Basin, Saudi Arabia. *Mar. Pet. Geol.* **2022**, *137*, 105495. [[CrossRef](#)]
20. Radwan, R.; Wood, D.; Mahmoud, M.; Tariq, Z. Gas adsorption and reserve estimation for conventional and unconventional gas resources. In *Sustainable Geoscience for Natural Gas Subsurface Systems*; Gulf Professional Publishing: Houston, TX, USA, 2022; Volume 2, pp. 345–382.
21. Sohail, G.; Radwan, A.; Mahmoud, M. A review of Pakistani shales for shale gas exploration and comparison to North American shale plays. *Energy Rep.* **2022**, *8*, 6423–6442. [[CrossRef](#)]
22. Zhang, Q.; Radwan, A.; Wang, K.; Liu, C.; Song, Z.; Lu, D.; Zhang, M.; Guo, C.; Yin, S. Pore structure characteristics of different lithofacies of the Longmaxi shale, Western Hunan-Hubei Region, China: Implications for reservoir quality prediction. *Geol. J.* **2023**, *27*, 1–10. [[CrossRef](#)]
23. Cheng, D.; Zhang, Z.; Hong, H.; Zhang, S.; Qin, C.; Yuan, X.; Zhang, B.; Zhou, C.; Deng, Q. Sequence structure, sedimentary evolution and their controlling factors of the Jurassic Lianggaoshan Formation in the East Sichuan Basin, SW China. *Pet. Explor. Dev.* **2023**, *50*, 262–271. [[CrossRef](#)]
24. He, W.; Bai, X.; Meng, Q.; Li, J.; Zhang, D.; Wang, Y. Accumulation geological characteristics and major discoveries of lacustrine shale oil in Sichuan Basin. *Acta Pet. Sin.* **2022**, *43*, 885–895.
25. Liu, H.; Li, J.; Liu, P.; Wang, X.; Wang, Y.; Qiu, Y.; Li, Z.; Wang, W. Enrichment conditions and strategic exploration direction of Paleogene shale oil in Jiyang Depression. *Acta Pet. Sin.* **2022**, *43*, 1717–1727. [[CrossRef](#)]
26. Baouche, R.; Sen, S.; Radwan, A. Geomechanical and Petrophysical Assessment of the Lower Turonian Tight Carbonates, Southeastern Constantine Basin, Algeria: Implications for Unconventional Reservoir Development and Fracture Reactivation Potential. *Energies* **2023**, *15*, 7901. [[CrossRef](#)]
27. Elsayed, M.; Isah, A.; Hiba, M.; Hassan, A.; Al-Garadi, K.; Mahmoud, M.; El-Husseiny, A.; Radwan, A. A review on the applications of nuclear magnetic resonance (NMR) in the oil and gas industry: Laboratory and field-scale measurements. *J. Pet. Explor. Prod. Technol.* **2022**, *12*, 2747–2784. [[CrossRef](#)]
28. Hakimi, M.; Hamed, T.; Lotfy, N.; Radwan, A.; Lashin, A.; Rahim, A. Hydraulic fracturing as unconventional production potential for the organic-rich carbonate reservoir rocks in the Abu El Gharadig Field, north western Desert (Egypt): Evidence from combined organic geochemical, petrophysical and bulk kinetics modeling results. *Fuel* **2023**, *334*, 126606.
29. GB/T 29172-2012; Practices for Core Analysis. National Standards of People’s Republic of China: Beijing, China, 2012.
30. GB/T18602-2001; Rock Pyrolysis Analysis. National Standards of People’s Republic of China: Beijing, China, 2012.
31. SY/T5118-2005; Determination of Bitumen from Racks by Chloroform Extraction. National Standards of People’s Republic of China: Beijing, China, 2012.
32. Ismail, A.; Din, M.; Radwan, A.; Gabr, M. Rock typing of the Miocene Hammam Faraun alluvial fan delta sandstone reservoir using well logs, nuclear magnetic resonance, artificial neural networks, and core analysis, Gulf of Suez, Egypt. *Geol. J.* **2023**, *16*, 1–10. [[CrossRef](#)]
33. He, H.; Peng, S.-P.; Shao, L.-Y. Trace elements and sedimentary settings of Cambrian-Ordovician carbonates in Bachu area, Tarim Basin. *Xinjiang Pet. Geol.* **2004**, *25*, 631.
34. Hu, X.M.; Wang, C.S. Several major geological events and global climate change since 100 Ma. *Exploration Nat.* **1990**, *18*, 53–58. [[CrossRef](#)]
35. Ni, Y.; Ma, Q.; Ellis, G. Fundamental studies on kinetic isotope fraction in natural gas systems. *Geochim. Cosmochim. Acta* **2011**, *75*, 2696–2707. [[CrossRef](#)]
36. Wang, J.; Wang, X. Seepage characteristic and fracture development of protected seam caused by mining protecting strata. *J. Min. Strat. Control Eng.* **2021**, *3*, 033511. [[CrossRef](#)]
37. Wang, H.; Zhou, S.; Li, S.; Zhao, M.; Zhu, T. Comprehensive characterization and evaluation of deep shales from Wufeng-Longmaxi Formation by LF-NMR technology. *Unconv. Resour.* **2022**, *2*, 1–11. [[CrossRef](#)]
38. Wang, P.; Liu, Z.; Zhang, D.; Li, X.; Liu, H.; Zhou, L.; Li, P. Source rock and reservoir qualities of middle Jurassic Liang-gaoshan lacustrine shale at fuxing area, Sichuan Basin: Implication for shale-oil enrichment. *Unconv. Resour.* **2023**, *3*, 37–43. [[CrossRef](#)]
39. Wang, S. Chemical characteristics of Jurassic-Sinian gasin Sichuan Basin. *Nat. Gas Ind.* **1994**, *14*, 1–5.
40. Xiao, J.F.; Hu, P.J.; Han, L.X. Mechanical properties and compressibility evaluation of Qiongzhusi shale in Weiyuan area in southern Sichuan. *Drill. Prod. Technol.* **2022**, *45*, 61–66. [[CrossRef](#)]

41. Yu, C.; Gong, D.; Huang, S. Geochemical characteristics of carbon and hydrogen isotopes for the Xujiahe Formation natural gas in Sichuan Basin. *Nat. Gas Geosci.* **2014**, *25*, 87–97.
42. Asante-Okyere, S.; Ziggah, Y.Y.; Marfo, S.A. Improved total organic carbon convolutional neural network model based on mineralogy and geophysical well log data. *Unconv. Resour.* **2021**, *1*, 1–8. [[CrossRef](#)]
43. Davies, G.R.; Smith, L.B. Structurally controlled hydrothermal dolomite reservoir facies—An overview. *J. AAPG Bull.* **2006**, *90*, 1641–1690. [[CrossRef](#)]
44. Guo, J.C.; Luo, B.; Zhu, H.Y. Evaluation of fracability and screening of perforation interval for tight sandstone gas reservoir in western Sichuan Basin. *J. Nat. Gas Sci. Eng.* **2015**, *25*, 77–87. [[CrossRef](#)]
45. Hao, B.; Hu, S.; Huang, S. Geochemical characteristics and its significance of reservoir bitumen of Longwangmiao Formation in Moxi area, Sichuan Basin. *Geoscience* **2016**, *30*, 614–626.
46. Hu, G.; Xie, Y. *Carboniferous Gas Fields in High Steep Structure of Eastern Sichuan*; Petroleum Industry Press: Beijing, China, 1997; pp. 47–62.
47. Mondal, S.; Chatterjee, R.; Chakraborty, S. An integrated approach for reservoir characterisation in deep-water Krishna-Godavari basin, India: A case study. *J. Geophys. Eng.* **2021**, *18*, 134–144. [[CrossRef](#)]
48. Li, J.; Li, H.; Yang, C.; Wu, Y.J.; Gao, Z.; Jiang, S.L. Geological characteristics and controlling factors of deep shale gas enrichment of the Wufeng-Longmaxi Formation in the southern Sichuan Basin, China. *Lithosphere* **2022**, *2022*, 4737801. [[CrossRef](#)]
49. Montgomery, S.L.; Jarvie, D.M.; Bowker, K.A. Mississippian Barnett shale, Fort Worth basin, north-central Texas: Gas shale play with multitrillion cubic foot potential. *AAPG Bull.* **2005**, *89*, 155–175. [[CrossRef](#)]
50. Ni, Y.; Liao, F.; Yao, L. Stable hydrogen isotopic characteristics of natural gas from the Xujiahe Formation in the central Sichuan Basin and its implications for water salinization. *Nat. Gas Geosci.* **2019**, *30*, 880–896. [[CrossRef](#)]
51. Wang, H.; Shi, Z.; Zhao, Q.; Liu, D.; Sun, S.; Guo, W.; Liang, F.; Lin, C.; Wang, X. Stratigraphic framework of the Wufeng-Longmaxi shale in and around the Sichuan Basin, China: Implications for targeting shale gas. *Energy Geosci.* **2020**, *1*, 124–133. [[CrossRef](#)]
52. Du, H.; Wang, W.; Shi, Z.; Tan, J.; Cao, H.; Yin, X. Geochemical characteristics and source of natural gas of the Upper Triassic Xujiahe Formation in Malubei area, northeastern Sichuan Basin. *Oil Gas Geol.* **2019**, *40*, 34–38. [[CrossRef](#)]
53. Fu, Y.; Jiang, Y.; Wang, Z. Non-connected pores of the Longmaxi shale in southern Sichuan Basin of China. *Mar. Pet. Geol.* **2019**, *110*, 420–433. [[CrossRef](#)]
54. Huang, J.; Chen, S.; Song, J. Sichuan Basin Hydrocarbon source system and the formation of large and medium-sized gas fields. *Sci. China D Series* **1996**, *26*, 504–510. [[CrossRef](#)]
55. Katz, B.; Gao, L.; Little, J.; Zhao, Y.R. Geology still matters—Unconventional petroleum system disappointments and failures. *Unconv. Resour.* **2021**, *1*, 18–38. [[CrossRef](#)]
56. Li, H. Research progress on evaluation methods and factors influencing shale brittleness: A review. *Energy Rep.* **2022**, *8*, 4344–4358. [[CrossRef](#)]
57. Liang, C.; Jiang, Z.X.; Zhang, C.M. The shale characteristics and shale gas exploration prospects of the Lower Silurian Long-maxi shale, Sichuan Basin, South China. *J. Nat. Gas Sci. Eng.* **2014**, *21*, 636–648. [[CrossRef](#)]
58. Mazumdar, C.; Alleno, E.; Sologub, O. Investigations of the structural, magnetic and Ce-valence properties of quaternary CeM2B2C compounds (M: Co, Ni Rh, Pd Ir and Pt). *ChemInform* **2003**, *34*, 18–25. [[CrossRef](#)]
59. Abraham-A, R.M.; Taioli, F.; Nzekwu, A.I. Physical properties of sandstone reservoirs: Implication for fluid mobility. *Energy Geosci.* **2022**, *3*, 349–359. [[CrossRef](#)]
60. Haas, J.; Hips, K.; Budai, T. Processes and controlling factors of polygenetic dolomite formation in the Transdanubian Range, Hungary: A synopsis. *J. Int. J. Earth Sci.* **2017**, *106*, 991–1021. [[CrossRef](#)]
61. Jiang, Y.; Gu, Y.; Li, K. Types and genesis of reservoir and permeability space of Middle Permian hydrothermal dolomite in the central Sichuan Basin. *Nat. Gas Ind.* **2018**, *38*, 16–24. [[CrossRef](#)]
62. Meyer, E.E.; Quicksall, A.N.; Landis, J.D. Trace and rare earth elemental investigation of a Sturtian cap carbonate, Pocatello, Idaho: Evidence for ocean redox conditions before and during carbonate deposition. *Precambrian Res.* **2013**, *192*, 89–106. [[CrossRef](#)]
63. Tian, Y.; Liu, S.; Zhao, Y. Formation mechanism of high quality reservoirs of Lower Cambrian Longwangmiao Formation in central Sichuan Basin. *J. Guilin Univ. Technol.* **2015**, *35*, 217–226.
64. Liang, Y.; Li, Y.; Fu, X.; Yuan, X.; Yang, J.; Zheng, J. Origin and whole hydrocarbon geochemical characteristics of oil and gas from Xujiahe group of Chuanzhong-Chuannan Transitional Belt. *Nat. Gas Geosci.* **2006**, *17*, 593–596. [[CrossRef](#)]
65. Lai, J.; Wang, G.W.; Wang, S.; Cao, J.T.; Li, M.; Pang, X.J.; Zhou, Z.L.; Fan, X.Q.; Dai, Q.Q.; Yang, L.; et al. Review of diagenetic facies in tight sandstones: Diagenesis, diagenetic minerals, and prediction via well logs. *Earth-Sci. Rev.* **2018**, *185*, 234–258. [[CrossRef](#)]
66. Mazzullo, S.J. Organogenic dolomitization in peritidal to deep-sea sediments. *J. Sediment. Res.* **2000**, *70*, 10–23. [[CrossRef](#)]
67. Qiu, Z.; Zou, C.; Wang, H. Discussion on the characteristics and controlling factors of differential enrichment of shale gas in the Wufeng-Longmaxi formations in south China. *J. Nat. Gas Geosci.* **2020**, *5*, 117–128. [[CrossRef](#)]
68. Saein, A.; Riahi, Z. Controls on fracture distribution in Cretaceous sedimentary rocks from the Isfahan region, Iran. *Geol. Mag.* **2017**, *156*, 1092–1104. [[CrossRef](#)]
69. Tang, L.; Song, Y.; Jiang, S. Sealing mechanism of the roof and floor for the Wufeng-Longmaxi shale gas in the southern Sichuan Basin. *Energy Fuels* **2020**, *34*, 6999–7018. [[CrossRef](#)]

70. Tan, K.; Yao, J.; Chen, J.; Tang, D.; Qin, Y.; Wu, Q. Controlling effect of source-reservoir assemblage on natural gas accumulation: A case study of the upper Triassic Xujiahe Formation in the Sichuan Basin. *Front. Earth Sci.* **2022**, *10*, 1028439. [[CrossRef](#)]
71. Vafaie, A.; Kivi, I.R.; Moallemi, S.A.; Habibnia, B. Permeability prediction in tight gas reservoirs based on pore structure characteristics: A case study from South Western Iran. *Unconv. Resour.* **2021**, *1*, 9–17. [[CrossRef](#)]
72. Yu, H.; Taleghani, A.D.; Lian, Z. On how pumping hesitations may improve complexity of hydraulic fractures, a simulation study. *Fuel* **2019**, *249*, 294–308. [[CrossRef](#)]
73. Zhang, D.W. Development prospect of natural gas industry in the Sichuan Basin in the next decade. *Nat. Gas Ind.* **2021**, *41*, 34–45. [[CrossRef](#)]
74. Nelson, P.H. Pore-throat sizes in sandstones, tight sandstones, and shales. *AAPG Bull.* **2009**, *93*, 329–340.

**Disclaimer/Publisher’s Note:** The statements, opinions and data contained in all publications are solely those of the individual author(s) and contributor(s) and not of MDPI and/or the editor(s). MDPI and/or the editor(s) disclaim responsibility for any injury to people or property resulting from any ideas, methods, instructions or products referred to in the content.